

# INVESTIGATION OF TRANSVERSE BEAM INSTABILITY INDUCED BY AN IN-VACUUM UNDULATOR AT SPEAR3\*

K. Tian<sup>†</sup>, J. Sebek, J. L. Vargas, SLAC National Accelerator Laboratory, Menlo Park, USA

## Abstract

Vertical beam instabilities have been observed at SPEAR3 when a newly installed in-vacuum undulator (IVUN) is operated at a set of narrow gap settings. The source of the instabilities is believed to be vertically deflecting trapped modes inside the IVUN tank that are excited by the beam. We have used beam-based measurements to characterize the frequencies and strengths of the excited modes using both our bunch-by-bunch feedback system and a spectrum analyzer. Using numerical simulations of our IVUN structure, we have found modes with high shunt impedance near the measured frequencies. Recently, we have successfully measured these IVUN modes during our current downtime. In this paper, we will report on the measurements, simulations, and plans to damp these modes.

## INTRODUCTION

Transverse beam instabilities at intermittent IVUN pole gap positions have previously been reported by other facilities [1-3]. However, the sources of the instabilities have never been well understood. Recently, we have observed similar beam instabilities associated with one of our IVUNs, the BL15 insertion device (ID).

The 2-meter-long BL15 insertion device in SPEAR3 is the second IVUN in the storage ring and is still under commissioning for full user operation. The undulator period is 22 mm with 86 full strength periods and 2 end periods with reduced strength. When in operations, it will close down to a minimum 6.82 mm pole gap. During early commissioning tests of BL15 ID, we encountered several problems. We found that the injection efficiency of the storage ring degraded significantly when the ID gap was closed to the minimum gap. Therefore, we temporarily raised the lower limit of the ID gap to 8 mm in the control system. Later, we found that the beam size blew up when the gap was set to 8.4 mm during 500mA operation. Upon further investigation, we have discovered that these problems are likely caused by vertical beam instabilities that have occurred at these and other intermittent pole gaps.

The cross section of the ID chamber is shown on the left of Fig. 1. As a standard means of decreasing the resistive wall impedance of the ID, two 70mm wide nickel-plated copper foils (current sheets) are attached to both the top and bottom rows of the magnets through the magnetic attractive force of the nickel to the pole pieces. Since the electron beam is shielded by the current sheet, we can simplify the complicated ID chamber assembly by

approximating it by a round ridge waveguide shown on the right of Fig. 1. The width and height of the narrow gap at the center of the ridge waveguide represent the width of the current sheets and the pole gap, respectively. Based on the theory of the ridge waveguide [4], the cutoff frequency of the waveguide will decrease with the gap height. Because the ID gap opens up to 34 mm at the end of the transition, a small gap means that the cut-off frequency for the cross-sections of the central part of the ID will be lower than that for the cross-sections at the ends of the ID. As a result, the beam can excite low frequency modes which are trapped inside the ID chamber. We believe that these trapped modes are the sources of the beam instabilities we observed at SPEAR3. In the following, we will present the results from beam based measurements, numerical simulations, and RF measurements to support our theory.

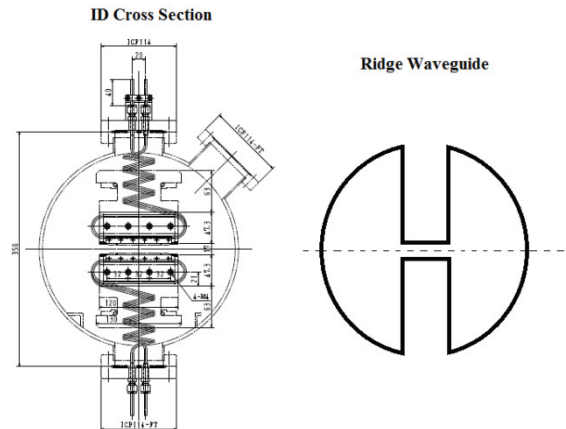


Figure 1: Cross section of SPEAR3 BL15 ID (left) and a round ridge waveguide (right).

## BEAM BASED MEASUREMENT

To reveal all the instability modes at different gaps, we scanned the ID gap from 6.82mm to 8.6mm at 10  $\mu\text{m}$  per step. Then we conducted modal analysis using the bunch-by-bunch (Bx B) data taken by the feedback system [5] to characterize the mode number and potential frequencies of the modes at different ID gaps. The results are shown in Table 1. The pole gap in the table is the rough midpoint for each instability mode. For the transverse beam instability, the lower betatron sideband drives the instability while the upper sideband damps it [6], so the instability modes and frequencies shown in the table all correspond to the lower sideband of the lowest potential driving frequency. Starting from 6.82mm, we observed a series of instability modes, each of which covered  $\sim$ 100  $\mu\text{m}$  gap range and was separated by  $\sim$ 300  $\mu\text{m}$  from its neighbors. This indicates that the resonant frequency of the problematic mode in the ID chamber reduces by one

\* Work supported by ý g'WJDOE.'QHeg'qh'Uelgpeg'wpf gt" contract

\*\* DE-AC02-76SF00515

† ktian@slac.stanford.edu

revolution frequency about every 300  $\mu\text{m}$  of gap closure, i.e.  $\sim 4.3$  MHz/mm.

Table 1: BL15 Pole Gap vs Instability Modes

Pole Gap(mm)	Peak Mode	Freq.( MHz)
6.82	156	199.51
7.10	157	200.79
7.43	158	202.07
7.77	159	203.35
8.10	160	204.63
8.40	161	205.91

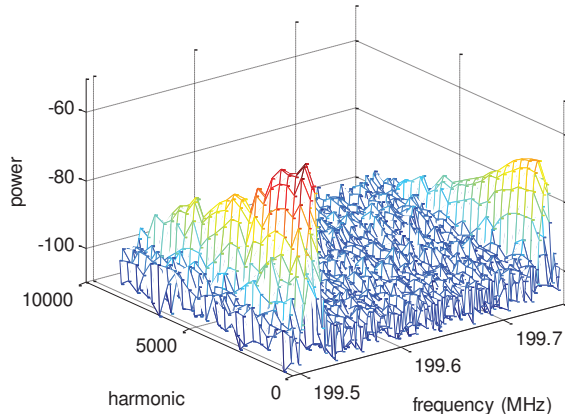


Figure 2: Spectrum analyzer data: pole gap at 6.82mm.

The frequencies of the beam instability modes at different pole gaps were also verified with an HP8563 spectrum analyzer monitoring a beam position monitor (BPM) button. During the experiment, we uniformly filled all RF buckets in order to suppress the revolution harmonics. For each instability mode, we set the analyzer span to just cover the revolution harmonic and the lower/upper side bands. Then we shifted the center frequency by the ring RF frequency, 476 MHz, to measure the same mode at the next higher candidate frequency. We continued these measurements up to about 10 GHz. Fig. 2 shows the results for mode 156 with the pole gap of 6.82mm and stored beam current of 191mA. In the figure, all frequencies have been aliased to the base band with the lower sidebands near 199.5 MHz and the revolution harmonics at 199.7 MHz. The lower sideband is obviously stronger than the revolution harmonic and the upper sideband (not shown here). These plots clearly show the unstable mode. However, from these measurements, we were unable to determine which of the aliased frequencies drove the instability.

## NUMERICAL SIMULATIONS

Numerical simulations for the possible modes causing the beam instabilities have been carried out using a parallel code, Omega3P [7], running on the super computer, Edison, at the National Energy Research Scientific Computing Center (NERSC) [8]. The solid model was build and meshed using CUBIT [9] and the data visualization was done with ParaView [10].

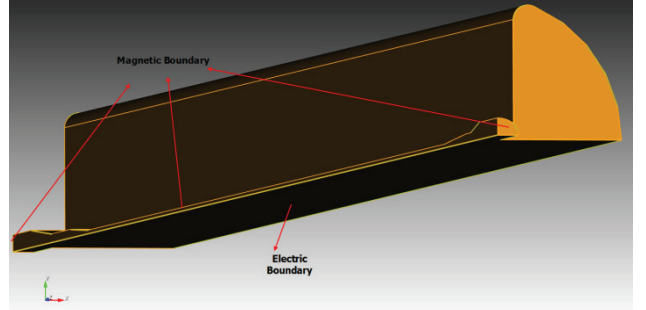


Figure 3: Solid model for the simulations.

Fig. 3 shows the solid model for the simulation, which is a quarter of the whole volume. The model is about 2.6 m long including 2 m of the ID length with transitions at both ends and about 60 cm for elliptical beam pipes having similar size as the standard SPEAR3 vacuum chamber. The full pole gap in this model is initially set to 7 mm. The center plane of the pole gap was set as an electric boundary so that only the TE modes were solved. Partitioning this problem into 22 run, we have spanned the spectrum up to 8 GHz and have found 4600 modes, with the computing time for each run from 10 minutes to 25 minutes.

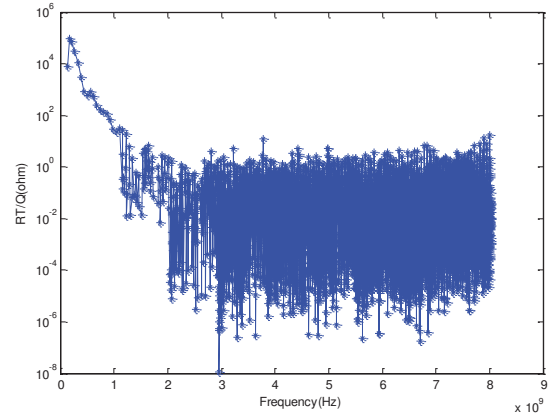


Figure 4: Transverse R/Q up to 8GHz at 7mm gap.

As shown in Fig. 4, the transverse R/Q of the modes above 1GHz are more than 4 orders of magnitude lower than those of the first 5 modes, which are all below 400 MHz. The results indicate that the trapped mode in the ID chamber causing the instability should be one of the low frequency modes and should have the same frequency as the instability mode. We have listed the transverse R/Q, Q, and the resonant frequencies for the first 6 modes in Table 2. In the simulation model, we did not include the ID magnets and other supporting mechanical structures, which can contribute significantly to the power dissipations of the resonant modes. As a result, the numerical solutions of the Q may have large discrepancies from the actual values. However, we still expect the mode frequencies and transverse R/Q to be reasonably accurate. At pole gap of 7 mm, our beam-based measurement tells us that the frequency of the instability mode is about 200 MHz. Therefore, Mode 3 in Table 2 is most likely to be the responsible mode because

it has a high transverse R/Q and is the closest resonant frequency to our measured value. Only Mode 2 showed a higher R/Q in the numerical simulations, but we did not observe instability at this Mode in SPEAR3.

Table 2: Simulation Results for the First 6 Modes

Mode ID	$(R/Q)_T$ (ohm)	Q	Freq.( MHz)
1	4.44085e+03	7439	136.48
2	6.15448e+04	4096	167.02
3	5.54048e+04	3127	212.38
4	2.52495e+04	2869	266.75
5	9.16657e+03	2860	325.91
6	2.80429e+03	2967	386.99

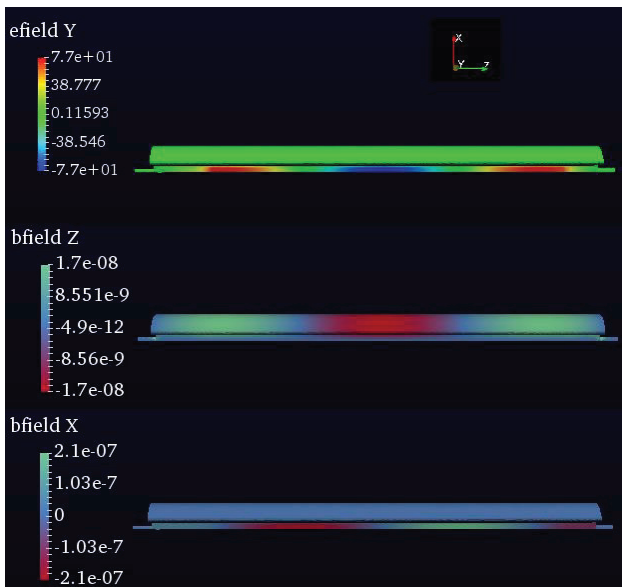


Figure 5: RF fields distribution of the 3<sup>rd</sup> mode. Top:  $E_y$ ; Middle:  $B_z$ ; Bottom  $B_x$ .

In the pole gap, the electromagnetic fields are dominated by the vertical electric field  $E_y$  and the horizontal magnetic field  $B_x$ . Elsewhere, in the vast volume of the rest of the ID chamber; the primary field is the longitudinal magnetic field  $B_z$ . For each Mode N in Table 2, the longitudinal variation of the RF fields goes through  $N/2$  periods in the chamber.

In Fig. 5, we illustrate the field distributions of the 3<sup>rd</sup> mode. Both  $E_y$  and  $B_z$  have a maximum at the longitudinal center while  $B_x$  has a null there. These symmetries also hold true for all the modes with odd numbers. For the even-numbered modes, the symmetries are exactly opposite:  $E_y$  and  $B_z$  vanish at the longitudinal center while  $B_x$  has its maximum there. The knowledge of the longitudinal RF field distributions of these modes is helpful for designing methods of coupling their power out of the chamber in an attempt to damp the unstable modes.

We then modified the model to change the pole gap to 6mm and 8mm, respectively, before repeating the simulation for the low frequency modes. The results are shown in Fig. 6. When varying the pole gap from 6mm to 8mm, the frequency of Mode 3 is varied by about 12 MHz, consistent with our beam-based measurements.

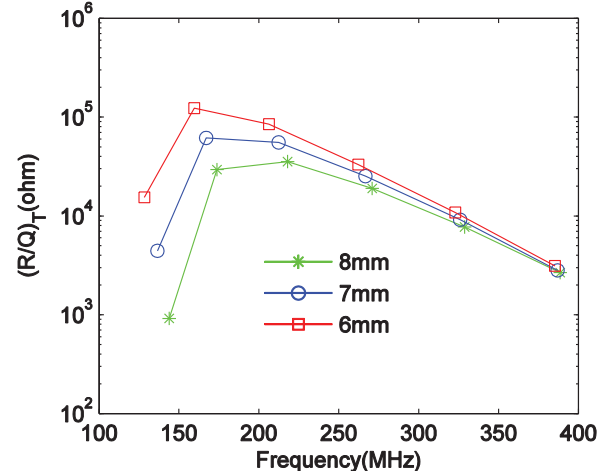


Figure 6: Simulation results at different gaps: 6mm, 7mm, and 8mm.

## RF MEASUREMENT

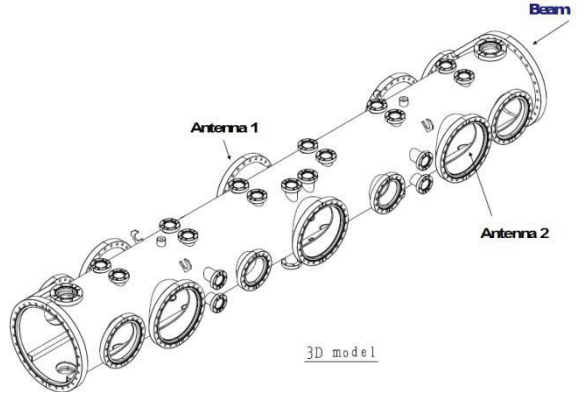


Figure 7: ID chamber and antennas locations.

During the recent SPEAR3 shutdown maintenance period, we conducted S parameter measurements of the BL15 chamber with an Agilent 8753ES network analyzer. We installed two loop antennas into the chamber, so that we could perform both  $S_{11}$  and  $S_{21}$  measurements. As shown in Fig. 7, one antenna is at the center port of the ID chamber and the other one is at an upstream port about 64.8 cm away. Both antennas are identical; each has a 94mm diameter loop connected to an N-type feedthrough. The loop size was maximized to have the coupling to the chamber as large as possible. However, for an RF frequency of about 200 MHz, the calculated free space radiation impedance from the antenna is only about  $0.3 \Omega$ , so we would expect relatively weak coupling for this measurement. Because, for Mode 3, the vacuum chamber is filled with nearly uniformly distributed longitudinal magnetic fields at the longitudinal center, the loop was placed vertically to maximize the coupling.

First we set the BL15 ID gap to 6.82mm and measured the return loss by monitoring the  $S_{11}$  at both ports. After scanning a wide range of frequency from 100 MHz to about 400 MHz, we found two dips at the center port corresponding to two modes. The first one was at 109 MHz with less than 0.1 dB return loss and the second one

was at about 200 MHz with about 0.2 dB return loss. Repeating the  $S_{11}$  measurement at the upstream port, the first dip became indistinguishable, but the dip at 200 MHz still remained. In addition another mode showed up at about 148 MHz. As indicated in the simulation, the longitudinal magnetic field has a maximum at the center of the ID chamber for Modes 1 and 3, but has a notch for Mode 2. Comparing the resonant frequency with the first three modes solved in Omega3P shown in Table 2, the discrepancy is reasonable. Therefore, we can conclude that the three modes we observed from the  $S_{11}$  measurements correspond to the first three modes in the numerical simulations.

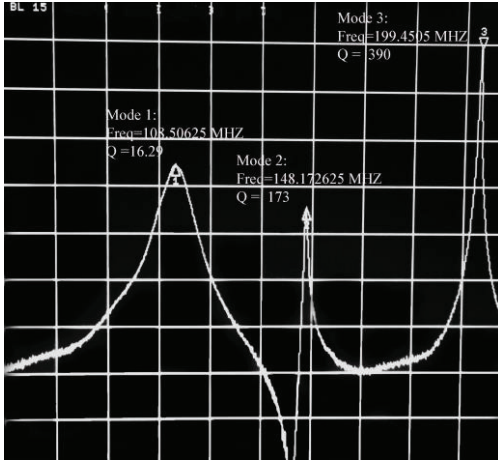


Figure 8:  $S_{21}$  measurement at two ports with 5dB/div.

As shown in Fig. 8, the first three resonant modes were all resolved clearly in the  $S_{21}$  measurements using both ports. By zooming into each peak, we can measure the  $Q$  for each mode as shown in Table 3.

Table 3:  $S_{21}$  Measurement Results for the First 3 Modes

Mode #	$Q$	Freq. (MHz)
1	16	108.51
2	173	148.17
3	390(0°)/388(45°)/380(90°)	199.45

For mode 3, we rotated the antenna at the center port from vertical orientation ( $90^\circ$ ) to diagonal ( $45^\circ$ ) and horizontal ( $0^\circ$ ) orientation. One should note that the rotation was not done precisely, so an error of several degrees can be expected. At  $0^\circ$ , the antenna had its weakest coupling to the mode, so the measured  $Q$  was close to the intrinsic  $Q$ . Table 3 shows that, at  $90^\circ$  (maximum coupling), the loaded  $Q$  only dropped by 10, less than 3% from the intrinsic  $Q$ , which suggests that the power coupled out of the chamber by the antenna is only a small fraction of the power loss inside the chamber. As a result, the antenna we installed for measurements will likely not be effective for coupling the trapped mode out of the chamber during the operation. Fig. 9 shows the measured resonant frequency of Mode 3 at various pole gaps from 6.82mm to 10mm at an interval of 0.1mm. The results fit a quadratic curve extremely well (following Slater's perturbation theory [11]) and also agree well with the frequencies of the beam instability mode.

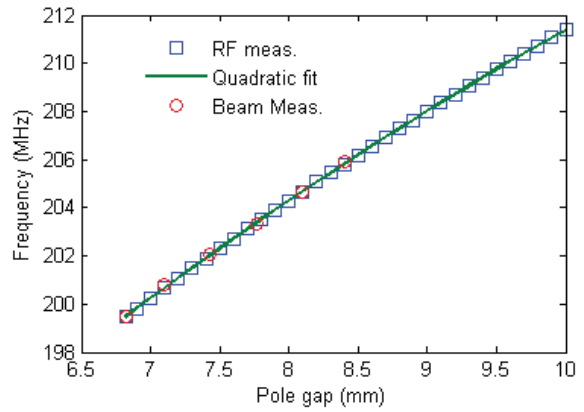


Figure 9: Frequency of Mode 3 at different gaps.

## CONCLUSION

After comprehensive studies on the beam instabilities induced by the BL15 ID, we believe that we have identified the trapped mode leading to the instabilities. We are working on the details of an engineering solution to damp the modes sufficiently for stable beam operation at SPEAR3. The results from the study will be useful for future IVUN development in SPEAR3.

## ACKNOWLEDGMENT

We want to thank Z. Li, J. Safranek, X. Huang, and A. Ringwall for useful discussions. We also want to thank members of the SSRL vacuum team and the SPEAR3 core team for their support in our RF measurements.

## REFERENCES

- [1] D. J. Peake *et al.*, "Preliminary Operational Experiences of a Bunch-by-bunch Transverse Feedback system at the Australian Synchrotron", in *Proc. IPAC'10*, Kyoto, Japan, May 2010.
- [2] R. Dowd *et al.*, "Investigations of Trapped Resonant Modes in Insertion Devices at The Australian Synchrotron", in *Proc. IPAC'16*, Busan, Korea, May 2016.
- [3] R. Bartolini *et al.*, "Analysis of multi -bunch instabilities at the Diamond storage ring", in *Proc. IPAC'16*, Busan, Korea, May 2016.
- [4] S. B. Cohn, "Properties of Ridge Wave Guide", in *Proceedings of the IRE* 35(8), 1947.
- [5] Dimtel, San Jose, USA, <http://www.dimtel.com>
- [6] A. Chao, *Physics of Collective Beam Instabilities in High Energy Accelerators*, John Wiley & Sons, Inc., 1993.
- [7] L.-Q. Lee *et al.*, "Omega3P: A Parallel Finite-Element Eigenmode Analysis Code for Accelerator Cavities", SLAC-PUB-13529, 2009.
- [8] NERSC website: <http://www.nersc.gov>
- [9] CUBIT code website: <https://cubit.sandia.gov>
- [10] ParaView code website: <http://www.paraview.org>
- [11] J. C. Slater, *Microwave Electronics*, Van Nostrand Company, Inc., 1950.